

# IMAGE RESTORATION AND RECONSTRUCTION USING VARIABLE SPLITTING AND CLASS-ADAPTED IMAGE PRIORS

Afonso M. Teodoro José M. Bioucas-Dias Mário A. T. Figueiredo

Instituto de Telecomunicações  
Instituto Superior Técnico, Universidade de Lisboa, Portugal

## ABSTRACT

This paper proposes using a Gaussian mixture model as a prior, for solving two image inverse problems, namely image deblurring and compressive imaging. We capitalize on the fact that variable splitting algorithms, like ADMM, are able to decouple the handling of the observation operator from that of the regularizer, and plug a state-of-the-art algorithm into the pure denoising step. Furthermore, we show that, when applied to a specific type of image, a Gaussian mixture model trained from a database of images of the same type is able to outperform current state-of-the-art methods.

**Index Terms**— Variable splitting, ADMM, Gaussian Mixture Model, Plug-and-Play, Image Reconstruction

## 1. INTRODUCTION

The classical linear inverse problem formulation of image reconstruction or restoration has the form

$$\mathbf{y} = \mathbf{A}\mathbf{x} + \mathbf{n}, \quad (1)$$

where  $\mathbf{y} \in \mathbb{R}^M$  denotes the observed data,  $\mathbf{x} \in \mathbb{R}^N$  is the (vectorized) underlying image to be estimated,  $\mathbf{A}$  is the observation matrix, and  $\mathbf{n}$  is noise (herein assumed to be Gaussian, with zero mean and known variance  $\sigma^2$ ). Typically, these problems are ill-posed, *i.e.*, there is no solution, or the solution is not unique, because  $\mathbf{A}$  is not invertible or is extremely ill-conditioned [1]. Consequently, these problems can only be solved satisfactorily if a regularizing term is introduced. This function, denoted  $\phi$ , is used to promote characteristics that the original image is known or assumed to have. A classical approach to tackling (1) with the help of  $\phi$  is by formulating an optimization problem of the form

$$\hat{\mathbf{x}} = \underset{\mathbf{x}}{\operatorname{argmin}} \frac{1}{2} \|\mathbf{A}\mathbf{x} - \mathbf{y}\|_2^2 + \alpha \phi(\mathbf{x}), \quad (2)$$

which combines a data-fidelity term with the regularizer, with parameter  $\alpha$  controlling their trade-off. To make problem (2) tractable, most of the work in this area has been focused on designing convex regularizers, such as the total-variation norm [2], which promotes piece-wise smoothness while maintaining sharp edges, or sparsity-inducing norms on wavelet transforms or representations [3].

Although countless optimization methods have been developed to address such problems, a lot of attention has been recently focused on variable splitting methods, such as the *alternating direction method of multipliers* (ADMM). Albeit proposed in the 70's [4], it is

a flexible and efficient tool, currently widely used to address imaging inverse problems [5], as well as in machine learning, and other areas. ADMM is able to deal with non-smooth convex regularization terms, it has good convergence properties, and it can be very efficiently implemented in a distributed way [6].

As mentioned above, the vast majority of work has focused on convex regularizers, due to their tractability. However, it is widely accepted today that the state-of-the-art methods for image denoising (*i.e.*, problems of the form (1) with  $\mathbf{A} = \mathbf{I}$ ) do not correspond to solving problems of the form (2) with a convex regularizer. In fact, most (if not all) of the best performing denoisers are patch-based (as pioneered in [7]) and use estimation tools such as collaborative filtering [8] or Gaussian mixture models (GMM) [9], [10]. Very recently, the integration of state-of-the-art denoisers in ADMM-based methods for imaging inverse problems has been proposed [11] (under the designation "plug-and-play priors"), by exploiting the ability of ADMM to decouple the handling of the observation operator from that of the regularizer.

In this paper, we extend the trend started in [11] in the following ways. Whereas [11] uses fixed denoisers, in this paper we use a GMM-based method [10], which opens the door to learning class-adapted denoisers (*e.g.*, for faces, text, fingerprints, or specific types of medical images). Although the idea of training denoisers for specific image classes has been very recently proposed [12], that work considers only pure denoising problems. In this paper, we show that by using a GMM-based denoiser plugged into the ADMM algorithm, we achieve state-of-the-art results in compressive image reconstruction [13], as well as in deblurring face and text images.

The paper is organized as follows. Section 2 briefly reviews how ADMM is used for deblurring and compressive imaging. Section 3 presents the adopted GMM-based denoiser. Section 4 reports the experimental results and Section 5 states some concluding remarks.

## 2. ADMM FOR IMAGE DEBLURRING AND RECONSTRUCTION

As the name suggests, splitting methods proceed by splitting the objective function and dealing with each term separately, yielding simpler optimization problems. It is straightforward to rewrite (2) as

$$\hat{\mathbf{x}} = \underset{\mathbf{x}}{\operatorname{argmin}} f_1(\mathbf{x}) + f_2(\mathbf{x}), \quad (3)$$

where  $f_1(\mathbf{x}) = \frac{1}{2} \|\mathbf{A}\mathbf{x} - \mathbf{y}\|_2^2$ , and  $f_2(\mathbf{x}) = \alpha \phi(\mathbf{x})$ . Introducing a new variable  $\mathbf{v}$ , such that  $\mathbf{x} = \mathbf{v}$ , the unconstrained problem (3) can be rewritten as a constrained one:

$$\hat{\mathbf{x}}, \hat{\mathbf{v}} = \underset{\mathbf{x}, \mathbf{v}}{\operatorname{argmin}} f_1(\mathbf{x}) + f_2(\mathbf{v})$$

*s.t.*  $\mathbf{x} = \mathbf{v}$ . (4)

This work was partially supported by the Portuguese *Fundação para a Ciência e Tecnologia* (FCT), grants UID/EEA/5008/2013 and BD/102715/2014.

The purpose of this splitting is that the constrained optimization problem may be easier to solve than the original one, namely via the augmented Lagrangian method (ALM), also known as the method of multipliers [14], [15]. The ALM proceeds by alternating between the minimization of the so-called augmented Lagrangian function

$$\hat{\mathbf{x}}, \hat{\mathbf{v}} = \underset{\mathbf{x}, \mathbf{v}}{\operatorname{argmin}} f_1(\mathbf{x}) + f_2(\mathbf{v}) + \mathbf{d}^T(\mathbf{x} - \mathbf{v}) + \frac{\mu}{2} \|\mathbf{x} - \mathbf{v}\|_2^2, \quad (5)$$

and updating the Lagrange multipliers  $\mathbf{d}$  (see below). In ADMM, the joint minimization in (5) is replaced by separate minimizations with respect to  $\mathbf{x}$  and  $\mathbf{v}$ , and a scaled version of the Lagrange multipliers is used. The resulting algorithm finally takes the form

$$\mathbf{x}^{k+1} := \underset{\mathbf{x}}{\operatorname{argmin}} f_1(\mathbf{x}) + \frac{\mu}{2} \|\mathbf{x} - \mathbf{v}^k - \mathbf{d}^k\|_2^2, \quad (6)$$

$$\mathbf{v}^{k+1} := \underset{\mathbf{v}}{\operatorname{argmin}} f_2(\mathbf{v}) + \frac{\mu}{2} \|\mathbf{x}^{k+1} - \mathbf{v} - \mathbf{d}^k\|_2^2, \quad (7)$$

$$\mathbf{d}^{k+1} := \mathbf{d}^k - (\mathbf{x}^{k+1} - \mathbf{v}^{k+1}). \quad (8)$$

Notice that (6) and (7) are, by definition, the *Moreau proximity operators* (MPO, see [16], [17]) of  $f_1$  and  $f_2$ , computed at  $\mathbf{v}^k + \mathbf{d}^k$  and  $\mathbf{x}^{k+1} - \mathbf{d}^k$ , respectively. Recall that the MPO of some convex function  $\psi$ , computed at some point  $\mathbf{z}$ , is given by

$$\operatorname{prox}_\psi(\mathbf{z}) = \underset{\mathbf{x}}{\operatorname{argmin}} \frac{1}{2} \|\mathbf{x} - \mathbf{z}\|_2^2 + \psi(\mathbf{x}). \quad (9)$$

The MPO (9) can be seen as the solution to a pure denoising problem, with  $\psi$  as the regularization function and  $\mathbf{z}$  as the noisy observations. There are several well-known proximity operators with closed-form, such as the *soft-threshold* function, which results from  $\psi(\mathbf{x}) = \|\mathbf{x}\|_1$ . For a comprehensive review, see [16], [17].

Instantiating ADMM with  $f_1(\mathbf{x}) = \frac{1}{2} \|\mathbf{A}\mathbf{x} - \mathbf{y}\|_2^2$ , and  $f_2(\mathbf{x}) = \alpha\phi(\mathbf{x})$  a convex regularizer, yields the SALSA algorithm [18]. In particular, (6) becomes a quadratic optimization problem, which has a linear solution given by:

$$\mathbf{x}^{k+1} = (\mathbf{A}^T \mathbf{A} + \mu \mathbf{I})^{-1} (\mathbf{A}^T \mathbf{y} + \mu \mathbf{z}). \quad (10)$$

As shown in [18], [19], this inversion can be done efficiently for several relevant classes of inverse problems, namely cyclic deblurring, inpainting, partial Fourier observations; more recently, it was shown that this inversion can also be efficiently done in non-cyclic deblurring [20]. In this paper, we will consider cyclic deblurring and compressive imaging.

### 2.1. Cyclic Deblurring

In the case of cyclic/periodic deblurring,  $\mathbf{A} \in \mathbb{R}^{N \times N}$  is a block circulant matrix, thus the inversion can be done in the 2D discrete Fourier domain. In fact, since  $\mathbf{A}$  is block circulant, it can be factored as  $\mathbf{A} = \mathbf{U}^H \mathbf{D} \mathbf{U}$ , where  $\mathbf{U}$  represents the 2D discrete Fourier transform matrix,  $\mathbf{U}^H = \mathbf{U}^{-1}$  is its inverse (with  $(\cdot)^H$  denoting conjugate transpose), and  $\mathbf{D}$  is a diagonal matrix. Consequently,

$$(\mathbf{A}^T \mathbf{A} + \mu \mathbf{I})^{-1} = (\mathbf{U}^H \mathbf{D} \mathbf{U} \mathbf{U}^H \mathbf{D}^H \mathbf{U} + \mu \mathbf{I})^{-1} = \mathbf{U}^H (|\mathbf{D}|^2 + \mu \mathbf{I})^{-1} \mathbf{U}.$$

The inversion of the diagonal matrix  $|\mathbf{D}|^2 + \mu \mathbf{I}$  has linear cost, and the multiplications by  $\mathbf{U}$  and  $\mathbf{U}^H$  can be done via the FFT algorithm.

### 2.2. Compressive Imaging

In compressive imaging [21], [13],  $\mathbf{A} \in \mathbb{R}^{M \times N}$  is a Gaussian measurement matrix, with  $M < N$ . The solution to (6) is again given by the  $N \times N$  inversion in (10), which becomes the bottleneck of the algorithm. Resorting to the matrix inversion lemma, it is possible to reduce the cost of the inversion by a factor of roughly  $(N/M)^3$ :

$$(\mathbf{A}^T \mathbf{A} + \mu \mathbf{I})^{-1} = \frac{1}{\mu} \left( \mathbf{I} - \mathbf{A}^T (\mathbf{A} \mathbf{A}^T + \mu \mathbf{I})^{-1} \mathbf{A} \right), \quad (11)$$

where the required inversion is now of size  $M \times M$ . Note, also, that this inversion is done only once, and can be precomputed and stored.

## 3. PLUG-AND-PLAY PRIORS

In this paper, instead of computing the MPO of some convex regularizer  $\alpha\phi$  in (7), we implement that step by using a state-of-the-art denoiser, as in [11], exploiting the fact that the MPO is itself a denoising function. Whereas [11] uses BM3D [8] and K-SVD [22], we take an alternative route and adopt GMM-based denoising [10], [9].

As shown in [10], clean image patches are well modelled by a GMM, which can be directly learned from the noisy image itself, using the expectation-maximization (EM) algorithm. With a GMM prior for the clean patches, the corresponding minimum mean squared error (MMSE) estimator can be obtained in closed-form [10]. In this paper, rather than learning the GMM prior from the observed data (which is not clear if it is possible in image deblurring, and even less so in compressive imaging), we propose to learn the GMM prior from a set of clean images. This approach opens the door to training a GMM denoiser on a specific class of images, aiming at achieving better reconstruction than with a generic denoiser.

The fact that a denoiser that may not correspond to the MPO of a convex regularizer is used to implement (7) makes the convergence of the resulting algorithm hard to analyse. In this paper, we refrain from theoretical convergence concerns, and focus only on the empirical performance of the method.

## 4. EXPERIMENTS

The proposed approach was tested on the two types of observation operators mentioned above (periodic convolution and compressive imaging). In addition to the proposed GMM denoiser, we also consider BM3D plugged into the ADMM algorithm. The experiments were carried out for the following four sets of images.

**Generic:** this dataset comprises several benchmark images, such *Lena* and *Cameraman*. The GMM-based denoiser starts by using a mixture estimated from five other benchmark clean images (*Hill*, *Boat*, *Couple*, *Peppers*, *Man*); after 100 iterations, a new GMM is obtained from the current image estimate. This update step aims at obtaining a GMM that is more adapted to the underlying image, and improves the final results.

**Text:** this dataset contains 10 images, available from the author of [12] (<http://videoprocessing.ucsd.edu/~eluo/>). One of them is selected as input image and all the others are used to train the GMM. Since the input image is from the same class as the images used for training, the mixture adaptation step is not performed.

**Faces:** this dataset is made of 100 face images of the same subject, obtained from the same source as the text images.

**Microsoft:** this dataset contains 591 images <http://research.microsoft.com/en-us/projects/objectclassrecognition/>.

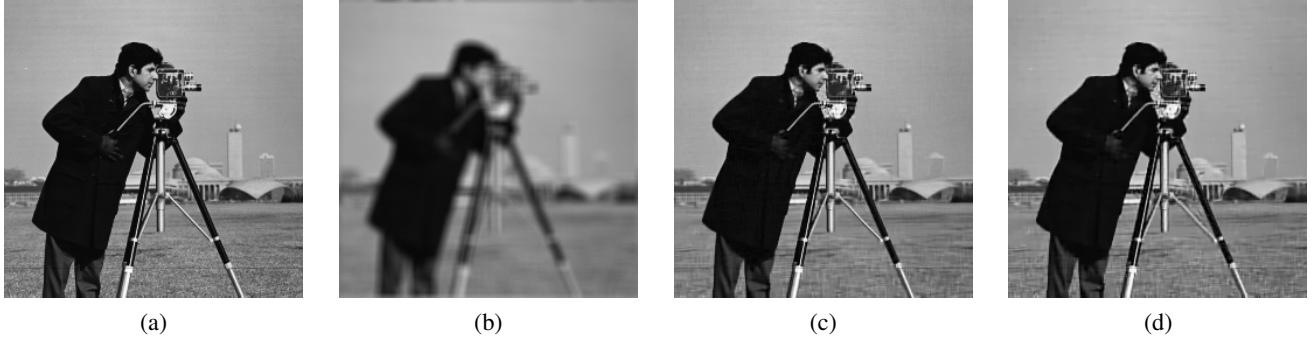


Fig. 1: Deblurring: (a) original Cameraman image; (b) blurred image (Experiment 3); (c) IDD-BM3D [23]; (d) ADMM-GMM.

Experiment	Cameraman						House					
	1	2	3	4	5	6	1	2	3	4	5	6
BSNR	31.87	25.85	40.00	18.53	29.19	17.76	29.16	23.14	40.00	15.99	26.61	15.15
Input PSNR	22.23	22.16	20.76	24.62	23.36	29.82	25.61	25.46	24.11	28.06	27.81	29.98
IDD-BM3D	<b>8.85</b>	<b>7.12</b>	<b>10.45</b>	<b>3.98</b>	<b>4.31</b>	4.89	<b>9.95</b>	<b>8.55</b>	12.89	<b>5.79</b>	<b>5.74</b>	7.13
BM3DDEB	8.19	6.40	8.34	3.34	3.73	4.70	9.32	8.14	10.85	5.13	4.56	7.21
ADMM-GMM	8.34	6.39	9.73	3.49	4.18	<b>4.90</b>	9.84	8.40	12.87	5.57	5.55	6.65
ADMM-BM3D	8.18	6.13	9.58	3.26	3.93	4.88	9.64	8.02	<b>12.95</b>	5.23	5.06	<b>7.37</b>

Experiment	Lena						Barbara					
	1	2	3	4	5	6	1	2	3	4	5	6
BSNR	29.89	23.87	40.00	16.47	27.18	15.52	30.81	24.79	40.00	17.35	28.07	16.59
Input PSNR	27.25	27.04	25.84	28.81	29.16	30.03	23.34	23.25	22.49	24.22	23.77	29.78
IDD-BM3D	7.97	<b>6.61</b>	8.91	<b>4.97</b>	<b>4.85</b>	6.34	7.64	<b>3.96</b>	<b>6.05</b>	1.88	1.16	5.45
BM3DDEB	7.95	6.53	7.97	4.81	4.37	6.40	<b>7.80</b>	3.94	5.86	<b>1.90</b>	1.28	<b>5.80</b>
ADMM-GMM	<b>8.01</b>	6.53	8.95	4.93	4.81	6.09	5.91	2.19	5.37	1.42	1.24	5.14
ADMM-BM3D	8.00	6.56	<b>9.00</b>	4.88	4.67	<b>6.42</b>	7.32	2.99	<b>6.05</b>	1.55	<b>1.40</b>	5.76

Table 1: ISNR on image deblurring. Methods: IDD-BM3D [23]; BM3DDEB [24]; ADMM with GMM and BM3D [8] denoising.

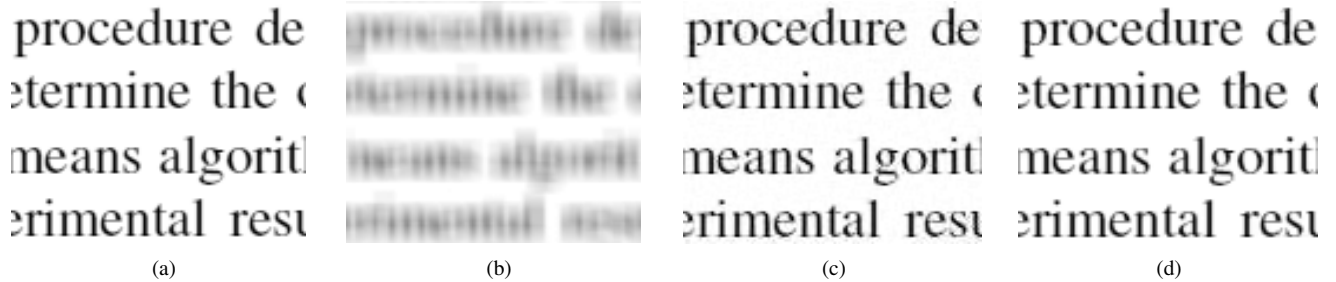
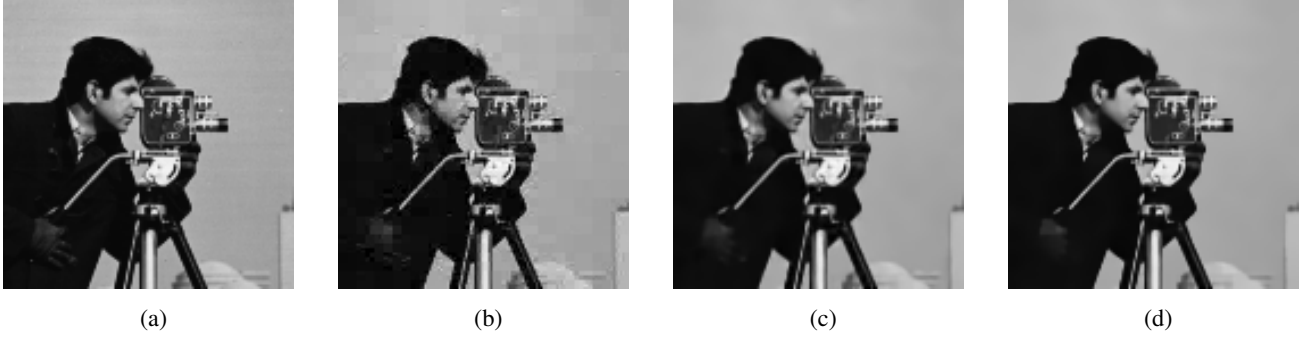


Fig. 2: Deblurring: (a) original Text image; (b) blurred image (Experiment 3); (c) IDD-BM3D [23]; (d) ADMM-GMM.

Experiment	Text						Face					
	1	2	3	4	5	6	1	2	3	4	5	6
BSNR	26.07	20.05	40.00	15.95	24.78	18.11	28.28	22.26	40.00	15.89	26.22	15.37
Input PSNR	14.14	14.13	12.13	16.83	14.48	28.73	25.61	22.54	20.71	26.49	24.79	30.03
IDD-BM3D	11.97	8.91	16.29	5.88	6.81	4.87	13.66	11.16	14.96	7.31	10.33	6.18
ADMM-GMM	<b>16.24</b>	<b>11.55</b>	<b>23.11</b>	<b>8.88</b>	<b>10.77</b>	<b>8.34</b>	<b>15.05</b>	<b>12.59</b>	<b>17.28</b>	<b>8.84</b>	<b>11.69</b>	<b>7.32</b>

Table 2: ISNR on image deblurring - Methods: IDD-BM3D [23]; ADMM with GMM prior and targeted databases.



**Fig. 4:** Compressive Imaging: (a) original image; (b) Turbo-GM (NMSE =  $-26.02$  dB) [13]; (c) ADMM-GMM without update (NMSE =  $-28.41$  dB) ; (d) ADMM-GMM with update (NMSE =  $-30.04$  dB)

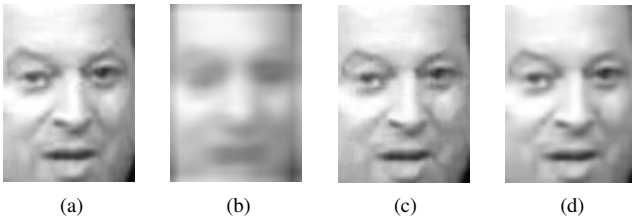


**Fig. 3:** Deblurring: (a) original Face image; (b) blurred image (Experiment 3); (c) IDD-BM3D [23]; (d) ADMM-GMM.

## 4.1. Results

### 4.1.1. Deblurring

The experiments were performed with the six different blur kernels available in the BM3D package (<http://www.cs.tut.fi/~foi/GCF-BM3D/index.html>). The results on the generic dataset are presented, both in terms of *improvement in SNR* (ISNR) and visual quality, in Table 1 and in Figure 1. The numbers relative to IDD-BM3D and BM3DDEB were obtained from [23], whereas the results of ADMM-BM3D were obtained by using the available implementation of BM3D in the ADMM loop, without any change. The results of the GMM prior were obtained using  $6 \times 6$  patches, and 20 components in the mixture. Other parameters of the algorithm, namely  $\mu$ , were hand tuned to provide the best results. The results (in Table 1) show that the proposed approach is competitive, yet does not beat IDD-BM3D [23] in this generic image deblurring experiment. Arguably, this may be due to the fact that some of the images being restored contain structures that are totally absent from the training set (e.g., the stripes on Barbara’s trousers or the pattern on the table cloth).

Concerning the problem of deblurring images of specific classes, the conclusion is very different. As shown in Table 2 and Figures 2 and 3, ADMM-GMM outperforms IDD-BM3D (using the default parameters) both visually and in terms of ISNR.

### 4.1.2. Compressive Imaging

With respect to compressive imaging, the same tests as in [13] were performed. Figure 4 compares the obtained results in terms of visual quality and normalized MSE (NMSE =  $\|\mathbf{x} - \hat{\mathbf{x}}\|_2^2 / \|\mathbf{x}\|_2^2$ ), showing that ADMM-GMM performs best. The algorithms were also run on all the images in the Microsoft dataset: as in [13], each image

was cropped to  $192 \times 192$ , starting from the top left corner, and then resized to  $128 \times 128$ . The number of measurements is  $M = 5000$ . The results are summarized in Figure 5 (a), clearly showing that for every image class, on average, ADMM-GMM performs best, by at least 2 dB. As in the deblurring case, the algorithm starts by using a generic mixture trained using images from the generic dataset, with 20 GMM components, and  $6 \times 6$  patches. The algorithm was run for 50 iterations on every image, with mixture update every 25 iterations. Finally, parameter  $\mu$  was kept fixed at 1. Figure 5 (b) shows how the NMSE changes with the number of measurements, using type 1 images from the Microsoft dataset.

Note: the Turbo-GM results were obtained by running the publicly available implementation with seed 0 on the random number generator, for comparison purposes. Although the results for Turbo-GM herein presented are slightly worse than those reported in [13], the difference does not affect our conclusion: on average, ADMM-GMM performs better than Turbo-GM.

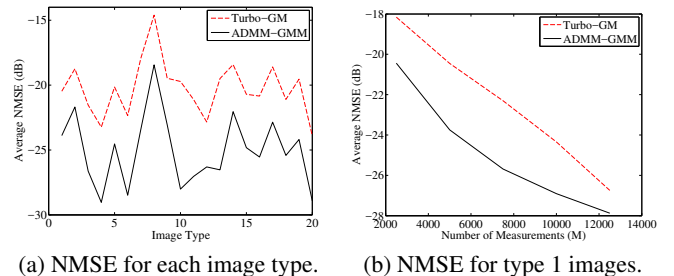


**Fig. 5:** NMSE comparison on compressive imaging.

## 5. CONCLUSIONS

This paper took advantage of some of the best priors for image denoising to address more complicated problems, such as deblurring and compressive imaging, by exploiting the fact that ADMM decouples the handling of the observation operator from the handling of the regularizer. In particular, we proposed using a GMM-based method in the denoising step, since it provides a framework for learning a class-specific denoiser. Indeed, the results show that using a GMM that is adapted to a given class of images, it is possible to improve the current state-of-the-art.

## 6. REFERENCES

- [1] M. Bertero and P. Boccacci, *Introduction to Inverse Problems in Imaging*, Institute of Physics Publishing, 1998.
- [2] L. Rudin, S. Osher, and E. Fatemi, “Nonlinear total variation based noise removal algorithms,” *Physica D: Nonlinear Phenomena*, vol. 60, pp. 259–268, 1992.
- [3] M. Elad, M. Figueiredo, and Y. Ma, “On the role of sparse and redundant representations in image processing,” *Proceedings of the IEEE*, vol. 98, no. 6, pp. 972–982, 2010.
- [4] D. Gabay and B. Mercier, “A dual algorithm for the solution of nonlinear variational problems via finite element approximation,” *Computers & Mathematics with Applications*, vol. 2, pp. 17–40, 1976.
- [5] M. Figueiredo and J. Bioucas-Dias, “Algorithms for imaging inverse problems under sparsity regularization,” in *Proceedings of the Workshop on Cognitive Information Processing (CIP 2012)*, 2012, pp. 1–6.
- [6] S. Boyd, N. Parikh, E. Chu, B. Peleato, and J. Eckstein, “Distributed optimization and statistical learning via the alternating direction method of multipliers,” *Foundations and Trends in Machine Learning*, vol. 3, pp. 1–122, 2011.
- [7] A. Buades, B. Coll, and J. Morel, “A non local algorithm for image denoising,” in *Proceedings of the IEEE Conference on Computer Vision and Pattern Recognition (CVPR 2005)*, 2005, vol. 2, pp. 60–65.
- [8] K. Dabov, A. Foi, V. Katkovnik, and K. Egiazarian, “Image denoising by sparse 3D transform-domain collaborative filtering,” *IEEE Transactions in Image Processing*, vol. 16, pp. 2080 – 2095, 2007.
- [9] G. Yu, G. Sapiro, and S. Mallat, “Solving inverse problems with piecewise linear estimators: From Gaussian mixture models to structured sparsity,” *IEEE Transactions on Image Processing*, vol. 21, no. 5, pp. 2481–2499, 2012.
- [10] A. Teodoro, M. Almeida, and M. Figueiredo, “Single-frame image denoising and inpainting using Gaussian mixtures,” in *4th International Conference on Pattern Recognition Applications and Methods*, 2015.
- [11] S. Venkatakrisnan, C. Bouman, E. Chu, and B. Wohlberg, “Plug-and-play priors for model based reconstruction,” in *Global Conference on Signal and Information Processing*, IEEE, 2013, pp. 945–948.
- [12] E. Luo, S. Chan, and T. Nguyen, “Adaptive image denoising by targeted databases,” *IEEE Transactions in Image Processing*, vol. 24, pp. 2167 – 2181, 2015.
- [13] S. Som, L. Potter, and P. Schniter, “Compressive imaging using approximate message passing and a Markov-tree prior,” in *Asiomatic Conference on Signals, Systems and Computers*. IEEE, 2010, pp. 243–247.
- [14] M. Hestenes, “Multiplier and gradient methods,” *Journal of Optimization Theory and Applications*, vol. 4, pp. 303–320, 1969.
- [15] M. Powell, “A method for nonlinear constraints in minimization problems,” in *Optimization*, R. Fletcher, Ed., pp. 283 – 298. Academic Press, 1969.
- [16] P. Combettes and V. Wajs, “Signal recovery by proximal forward-backward splitting,” *SIAM Journal on Multiscale Modeling & Simulation*, vol. 4, pp. 1168–1200, 2005.
- [17] P. Combettes and J-C. Pesquet, “Proximal splitting methods in signal processing,” in *Fixed-point Algorithms for Inverse Problems in Science and Engineering*, pp. 185–212. Springer, 2011.
- [18] M. Afonso, J. Bioucas-Dias, and M. Figueiredo, “Fast image recovery using variable splitting and constrained optimization,” *IEEE Transactions on Image Processing*, vol. 19, pp. 2345–2356, 2010.
- [19] M. Afonso, J. Bioucas-Dias, and M. Figueiredo, “An augmented Lagrangian approach to the constrained optimization formulation of imaging inverse problems,” *IEEE Transactions on Image Processing*, vol. 20, pp. 681 – 695, 2011.
- [20] M. Almeida and M. Figueiredo, “Deconvolving images with unknown boundaries using the alternating direction method of multipliers,” *IEEE Transactions on Image Processing*, vol. 22, pp. 3084 – 3096, 2013.
- [21] J. Romberg, “Imaging via compressive sampling,” *IEEE Signal Processing Magazine*, vol. 25, pp. 14–20, 2008.
- [22] M. Aharon, M. Elad, and A. Bruckstein, “K-SVD: An algorithm for designing overcomplete dictionaries for sparse representation,” *IEEE Transactions in Signal Processing*, vol. 11, pp. 4311 – 4322, 2006.
- [23] A. Danielyan, V. Katkovnik, and K. Egiazarian, “BM3D frames and variational image deblurring,” *IEEE Transactions in Image Processing*, vol. 21, pp. 1715 – 1728, 2012.
- [24] A. Danielyan, V. Katkovnik, and K. Egiazarian, “Image deblurring by augmented Lagrangian with BM3D frame prior,” *Workshop on Information Theoretic Methods in Science and Engineering*, 2010.